

## Integrated front–rear-grid optimization of free-form solar cells

Gupta, Deepak; Barink, M; Galagan, Y; Langelaar, Matthijs

**DOI**

[10.1109/JPHOTOV.2016.2617082](https://doi.org/10.1109/JPHOTOV.2016.2617082)

**Publication date**

2016

**Document Version**

Accepted author manuscript

**Published in**

IEEE Journal of Photovoltaics

**Citation (APA)**

Gupta, D., Barink, M., Galagan, Y., & Langelaar, M. (2016). Integrated front–rear-grid optimization of free-form solar cells. *IEEE Journal of Photovoltaics*, 7 (2017)(1), 294-302.  
<https://doi.org/10.1109/JPHOTOV.2016.2617082>

**Important note**

To cite this publication, please use the final published version (if applicable).  
Please check the document version above.

**Copyright**

Other than for strictly personal use, it is not permitted to download, forward or distribute the text or part of it, without the consent of the author(s) and/or copyright holder(s), unless the work is under an open content license such as Creative Commons.

**Takedown policy**

Please contact us and provide details if you believe this document breaches copyrights.  
We will remove access to the work immediately and investigate your claim.

# Integrated front-rear grid optimization of free-form solar cells

Deepak K. Gupta<sup>1</sup>, Marco Barink<sup>2</sup>, Yulia Galagan<sup>3</sup>, and Matthijs Langelaar<sup>1</sup>

<sup>1</sup>Department of Precision and Microsystems Engineering, Delft University of Technology, 2628CD Delft, The Netherlands, e-mail: D.K.Gupta@tudelft.nl, M.Langelaar@tudelft.nl.

<sup>2</sup>M. Barink is with TNO/Holst Centre, High Tech Campus 31, 5605KN Eindhoven, The Netherlands, email: Marco.Barink@tno.nl.

<sup>3</sup>Y. Galagan is with the Holst Centre - Solliance, High Tech Campus 21, 5656AE Eindhoven, The Netherlands, email: Yulia.Galagan@tno.nl.

Friday 7<sup>th</sup> October, 2016

## Abstract

Free-form solar cells expand solar power beyond traditional rectangular geometries. With the flexibility of being installed on objects of daily use, they allow making better use of available space and are expected to bring in new possibilities of generating solar power in the coming future. In addition, their customizable shape can add to the aesthetics of the surroundings. Evidently, free-form solar cells need to be efficient as well. One way to improve their performance is to optimize the metallization patterns for these cells. This work introduces an optimization strategy to optimize the metallization designs of a solar cell such that its performance can be maximized. For the purpose of optimization, we model an existing transparent free-form solar cell design, including front and rear electrode patterns, to validate it against previously published experimental results. The front and rear metallizations of this transparent free-form solar cell are subsequently redesigned using topology optimization. More than 50% improvement in output power is achieved by using topology optimization.

## 1 Introduction

With the growing energy demand and the need for new and clean energy resources, solar power is experiencing remarkable growth throughout the world. It is expected that the cumulative global solar photovoltaics (PV) market will triple to around 700 GW in 2020 compared to that in 2015 [1] and a long-term global forecast scenario describes worldwide solar PV capacity to reach 4600 GW by 2050 [2]. Looking at the United States alone, the total electrical power sector capacity in 2015 was reported to be around 1045 GW [3] with 27 GW of total solar power capacity and it is reported that 30% of its all new electricity generation capacity in 2015 came from solar [4]. In 2016, the PV installations are expected to increase by around 65 GW.

To ensure that solar power can be a sustainable solution to the growing energy demand for future, innovative ways are being explored to increase the overall PV installations. In some recent works, free-form solar cells have been designed which can be installed on objects of daily use [5–7]. These provide new possibilities of generating solar power, however, the generated energy needs to be affordable as well. Significant research is being conducted to make solar cells more efficient and thereby reduce the cost per unit of solar energy [8].

Among various other possibilities to enhance efficiency is optimization of solar cell metallization patterns. The metallization determines the voltage distribution over the cell, which affects the generated current and power. Significant research has been conducted in the past to improve on this aspect [9–13]. To the best of our knowledge, these standard methods are restricted to predefined geometries such as the H-pattern and in general optimize for the grid width and the spacing between the grid lines. The truly optimal designs might be more complex than the shapes that can be realized from optimization under such restrictions. With the advancements in printing technologies, fabricating more complex patterns is no longer a problem [7, 14],

however, the real challenge lies in designing them such that the solar cell performance can be improved.

In a paper presented at the 40th IEEE Photovoltaic Specialists Conference [15], it was shown that new and potentially superior layouts can be generated using a topology optimization (TO) approach. TO is a computational paradigm capable of optimizing the distribution of a certain material in a given domain subjected to certain constraints, such that the performance of the system is maximized [16]. Compared to conventional shape and size optimization approaches, TO provides more flexibility and does not even require an initial design concept. For a general overview of the concepts and applications of TO, see [16–18] and references therein. In the context of solar cells, TO has also been used to design efficient light trapping structures [19–21].

The work presented in [15] uses TO to optimize the front metallization patterns for solar cells. The details related to the mathematical formulation of the problem as well as the computational aspects of the methodology are discussed in [22]. It is also shown that the optimized front metal grids obtained using TO are comparable in terms of performance to the H-patterns for standard solar cell shapes.

An important advantage of the TO methodology is demonstrated in [23], where this method is used to optimize the front metal grids for *free-form, non-rectangular* solar cells. Freeform solar cells are gaining recent attention from an aesthetic point of view since they can easily blend into the architectural makeup of the surroundings. For recent research related to unconventional shapes for the solar cell domain, see [5–7, 23, 24]. In the study reported in [23], front grid patterns for several freeform shapes were optimized *e.g.* circular, hexagonal, leaf-shaped, shapes of motorbike fairings, *etc.* For unconventional shapes, no established efficient grid pattern is known, like the H-pattern for rectangular cells. Grid optimization using the TO approach however applies to any domain shape.

It is important to note here that while TO can design efficient metallization patterns for freeform solar cells, there are various other challenges associated with these freeform shapes. Manufacturing non-rectangular solar cell shapes (*e.g.* circular or semi-circular geometries) and the corresponding grid layouts has been attempted for the past four decades [25]. Manufacturing of free-form silicon solar cells is quite difficult due to technological limitations. Printing and coating techniques utilized in the manufacturing of organic solar cells open a lot of possibilities in the freedom of forms and shapes. These create a new market for PV technologies by combining PV functionality and aesthetics. Therefore, solar cells with artistic shapes attract a lot of attention. However, scaling up the size and their non-rectangular shapes typically lead to efficiency losses. It points on the necessity of optimization the metallization patterns for these cells.

In conventional solar cells, only the front electrode has been considered for optimization, as the rear electrode usually covers the entire backside. Transparent or semi-transparent solar cells are more aesthetically appealing than the opaque ones. To preserve this transparency, it is important not to cover the whole rear surface with the electrode material. Thus, a limited amount of electrode material can be used on the rear side and it becomes important to use an appropriate pattern. Important to note here is that the optimal grid designs for the front and the rear sides depend on each other, since together they determine the local voltage difference between front and rear side that determines the local current density. To maximize the performance of a solar cell, they should be optimized together. Some preliminary results related to this aspect were reported by us in [26], however that study was restricted to only electrode thickness optimization on the rear side.

This paper presents for the first time an optimization strategy which can be used to simultaneously optimize the front and rear metallization patterns for solar cells. For the purpose of this optimization, a solar cell model with front and rear metal designs is presented. Based on the available experimental data, the model is tuned so as to match the behavior of the fabricated tree-shaped solar cell example presented in [7]. Further, this model together with the proposed approach are used to optimize the metallization designs for this example.

The rest of this paper is organized in the following manner. Section 2 describes the optimization method and the mathematical model for the integrated front-rear grid optimization in solar cells. This approach is tested on a solar cell with the shape of a Christmas tree. The model validation and optimization results are discussed in Section 3 and the final conclusions are presented in Section 4.

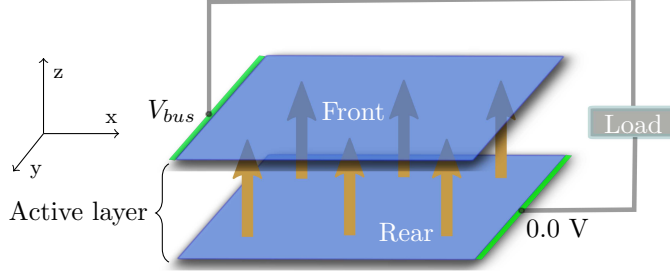


Figure 1: Schematic diagram of a solar cell model with front and rear conductive surfaces. The voltage difference between the front and rear sides, combined with the illumination level, controls the current density across any point in the semiconductor layer.

## 2 Method

### 2.1 Topology Optimization

In this work, topology optimization (TO) is used to simultaneously optimize the front and rear metallization patterns for solar cells. As stated above, TO is a computational approach capable of optimizing the material distribution in a given domain without violating some given constraints such that the performance of the system is maximized. In the traditional optimization methods, the electrode pattern is assumed to consist of straight lines and the design is only optimized for metal line width and line spacing. TO abandons such restrictions and can achieve more complex and better performing designs which cannot be obtained with the conventional shape optimization techniques.

TO comprises of a series of design updates, each update being based on the sensitivity responses computed from the design obtained in the previous step. Typically, the design domain at each step is discretized into a set of finite elements and the performance of the design is evaluated using finite element analysis. Within every finite element, the amount of material is allowed to vary from 0 to 1. Here 0 refers to void (no material) and 1 refers to solid (full material). To obtain a manufacturable solution, the intermediate values are penalized and made unfavorable [27, 28]. The optimization process is stopped when changes in objective value or design fall below a certain threshold in consecutive steps.

### 2.2 Mathematical formulation

In this section, the mathematical aspects of the solar cell metallization design optimization problem are discussed. A solar cell model with front and rear electrodes is presented and then the various aspects of the proposed optimization strategy are discussed. These are as follows:

#### 2.2.1 Solar cell model

For the purpose of front and rear grid optimization in solar cells, a simplified model is used. This model is an extended version of the front grid optimization model described in [22] and is illustrated in Fig. 1. In this figure, the semiconductor layer is sandwiched between the front and rear conductive surfaces. In general, these surfaces might consist of thin, transparent, moderately conductive layers with a deposition of highly conductive metal grid lines. Since the conductivity of the transparent layers as well as the metal grid is several orders higher than that of the active layer, it is assumed that the current across the active layer in the thin-film solar cell travels in the transverse direction. On the front and rear conductive surfaces, current flows along the surface planes.

The out-of-plane current density at any spot of the solar cell can be described using the following equation:

$$J = J_L - J_0(e^{\frac{q\Delta V}{k_B T}} - 1), \quad (1)$$

where  $J$ ,  $J_0$  and  $J_L$  denote net, reverse bias and photoillumination current densities, respectively and  $q$ ,  $k_B$  and  $T$  refer to the electric charge, Boltzmann constant and local temperature, respectively. In general,  $J_L$

does not depend on the voltage difference as in Eq. 1. However, for organic solar cells, Eq. 1 does not fit very well [31–33]. While modeling, this needs to be taken into account and the behavior of the device needs to be accurately modeled. The illumination can be non-uniform on the solar cell front surface, however, here we consider uniform illumination only. The voltage difference across the active layer denoted by  $\Delta V$  is equal to  $V_f - V_r$ , where  $V_f$  and  $V_r$  denote the voltage values measured on the front and rear conductive surfaces, respectively. For the front side, the busbar voltage is denoted by  $V_{bus}$  and on the rear side, the point at which the load is connected is set to 0 volts. The power output can then be stated as

$$P_{out} = (V_{bus} - 0) \int_{\Omega} J dA = V_{bus} \int_{\Omega} J dA. \quad (2)$$

Here,  $dA$  is a differential area of the solar cell and  $J$  is the respective out-of-plane current density. The efficiency  $\eta$  of the solar cell can then be calculated as

$$\eta = \frac{P_{out}/A}{p_{inp}} \times 100\%, \quad (3)$$

where  $P_{out}$  and  $A$  refer to the solar cell power output and its front surface area and  $p_{inp}$  is the input power density which is assumed to be  $100 \text{ mWcm}^{-2}$  under standard conditions.

### 2.2.2 Finite element modelling

The physics of the front as well as the rear conducting layers can be modelled using a Poisson equation of charge conservation during electrical conductivity, which is as follows:

$$\sigma \Delta^2 V = -\frac{\partial \rho}{\partial t}, \quad (4)$$

where  $\sigma$ ,  $V$  and  $\rho$  refer to the conductivity of the material, the electric potential and the enclosed charge density, respectively. When discretised using finite element method, the system of equations for the front and rear sides combined together can be stated as

$$\mathbf{G}\mathbf{V} = \mathbf{I}, \quad (5)$$

where  $\mathbf{G}$  is the total conductivity matrix and  $\mathbf{V}$  and  $\mathbf{I}$  refer to voltage and current vectors, respectively. From Eq. 1, it can be seen that the current and voltage are non-linearly related. Due to this, the system of equations given in Eq. 5 cannot be solved directly. Thus, it is transformed into a set of residual equations and then the system is solved to minimize the overall residual using the Newton method. Changing Eq. 5 to a residual form, the following can be stated:

$$\mathbf{R}(\mathbf{V}) = \mathbf{G}\mathbf{V} - \mathbf{I}(\mathbf{V}) = \mathbf{0}, \quad (6)$$

where  $\mathbf{R}$  is the residual. For the discretized system, quadrilateral finite elements with bilinear shape functions are used. The total conductivity matrix  $\mathbf{G}$  is constructed from the element conductivity matrix  $\mathbf{G}^{(e)}$  using a modified SIMP model [27] as follows:

$$\mathbf{G}^{(e)} = (G_{min} + \tilde{x}^p(G_0 - G_{min}))\mathbf{G}_0^{(e)}, \quad (7)$$

where  $G_{min}$  and  $G_0$  are linear conductivities of the transparent conductive layer and the metal electrode, respectively and  $\tilde{x}$  denotes the fraction of the finite element filled with the electrode material. The term  $p$  refers to penalization power and for this problem it is set to 3. This serves to obtain clearly resolved electrode designs. For more details on this aspect, see [22].

The various components of Eq. 6 are constructed as follows:

$$\mathbf{R} = [\mathbf{R}_f \quad \mathbf{R}_r]^T, \quad (8)$$

$$\mathbf{V} = [\mathbf{V}_f \quad \mathbf{V}_r]^T, \quad (9)$$

$$\mathbf{G} = \begin{bmatrix} \mathbf{G}_f & 0 \\ 0 & \mathbf{G}_r \end{bmatrix}, \quad (10)$$

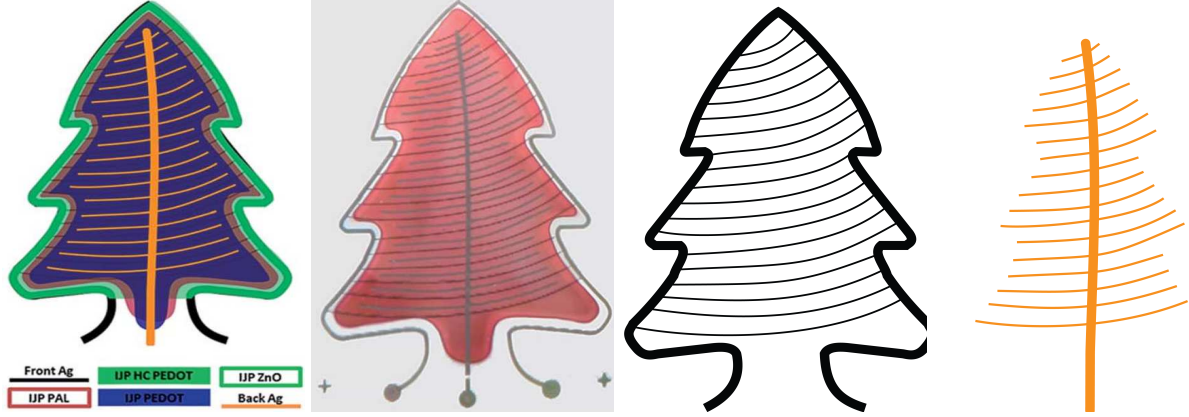


Figure 2: Christmas tree shaped free-form solar cell, (a) schematic diagram showing the layout of different printed layers [7] (b) photograph of the solar cell fabricated using inkjet printing [7] (c) modeled front side metallization design and (d) modeled rear side metallization design.

where, the subscripts  $f$  and  $r$  correspond to the front and rear surfaces of the solar cell, respectively. The global conductivity matrices  $\mathbf{G}_f$  and  $\mathbf{G}_r$  can be constructed by assembling the contributions from element conductivity matrices for the front and rear grids, respectively. For the consistency of the model, it is important that the magnitude of current entering the active layer at any spot on the rear side is equal to the current exiting the active layer from the corresponding spot on the front side. Thus,  $\mathbf{I}$  is constructed as follows:

$$\mathbf{I} = [\mathbf{I}_0 \quad -\mathbf{I}_0]^T. \quad (11)$$

The model proposed in [22] for the front side metallization assumes that the current flows from the whole front surface to the connection point (busbar). However, for the rear side, current needs to flow from the connection point to the whole rear surface. To take this into account, a minus sign is added to the current vector for the rear side.

### 2.2.3 Optimization

The objective of optimizing the metallization patterns is to maximize the solar cell efficiency. The mathematical formulation of the optimization problem can be stated as

$$\begin{aligned} & \max_{\tilde{\mathbf{x}}, V_{bus}} \eta \\ & \mathbf{R}(\mathbf{V}) = \mathbf{G}\mathbf{V} - \mathbf{I}(\mathbf{V}) = \mathbf{0}, \\ & \frac{1}{N} \sum \tilde{x}_r \leq V_r. \end{aligned} \quad (12)$$

Here,  $\tilde{\mathbf{x}}$  is given as  $\tilde{\mathbf{x}} = [\tilde{\mathbf{x}}_f \quad \tilde{\mathbf{x}}_r]$ , where  $\tilde{\mathbf{x}}_f$  and  $\tilde{\mathbf{x}}_r$  are the vectors of design variables for the front side and rear side, respectively and  $V_r$  denotes the material volume fraction for the rear side. Each design variable denotes the volume fraction of the finite element filled with the electrode material. The inequality constraint in Eq. 12 represents the restriction on the maximum amount of electrode material that can be used on the rear side of the solar cell. We also let the optimizer find the optimal busbar voltage  $V_{bus}$ , by including it as a design variable in the optimization problem.

For the front side of the solar cell, it is important that an optimum amount of electrode material is chosen. For too less material, the resistive losses will be high due to the increased contrast in voltage distribution on the front side. If too much material is used, although the resistive losses are reduced, a significant part of the incident light gets blocked from entering the active layer leading to increased shading losses. Between the two cases, there exists an optimum amount of material which reduces the sum of the two losses and this can be determined by the optimizer. Thus, unlike the rear side, no restriction needs to be imposed on the

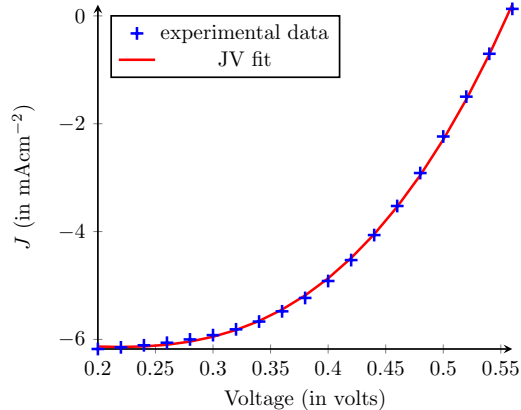


Figure 3: J-V data measured for a small device ( $0.04 \text{ cm}^2$ ) and the fitted J-V curve (obtained using a cubic polynomial) for the OPV solar cell used in this study.

maximum allowable amount of front electrode material. The shading effect is taken into consideration by replacing  $J_L$  in Eq. 1 by  $J_L^*$  such that

$$J_L^* = J_L(1 - \tilde{x})^r, \quad (13)$$

where  $r$  is a penalization power which is set to 2 in this study, to promote well-defined 0/1 solutions.

The optimization problem stated in Eq. 12 is a nonconvex optimization problem with more than 300,000 design variables and is solved using a gradient based technique. The model generated at each iteration step is updated using method of moving asymptotes [29], a gradient based optimizer capable of handling general non-linear programming problems with large number of design variables. For making a design update, the optimizer needs design sensitivities *i.e.* gradient information denoting the dependence of cell efficiency on the design. Due to the high dimensionality of the problem, an adjoint formulation is adopted for calculating these sensitivities [22, 30].

### 2.3 Applications

In this work, we use TO to optimize the front and rear metallizations for free-form solar cells. To demonstrate the applicability of TO, a free-form Christmas tree shaped organic photovoltaic (OPV) cell domain is chosen. One of the reasons to choose this test case is the fact that a similar OPV has been fabricated in the past and the results are reported in [7]. Since the goal of the paper is to present the optimization methodology, the choice of the test case does not limit the application of the methodology. Also, OPV and the inkjet printing technology have a big advantage compared to c-Si due to the possibility of freeforms. These give enormous aesthetical advantage and open possibility for new applications.

Here, we model the electrical behaviour of this test case as it is in [7] using the proposed front-rear electrode model. The model is tuned based on the available experimental data so that it can match the behavior of the fabricated solar cell example. The front and rear metallization patterns are then optimized under two different scenarios assuming that the amount of electrode material that can be used on the rear side is same (12%) as that in [7]. For the first case, the busbar on the front side is assumed to be the same as that in [7] and the electrode distribution is optimized for the rest of the front domain as well as on the rear side. For the second case, no pre-defined busbar configuration is assumed and TO is used to design efficient patterns for both the sides. For both the cases, the busbar connection points on the front and rear sides are assumed to be same as that in [7]. In addition, TO is also used to study the effect of amount of rear electrode material on the performance of the solar cell.

## 3 Results and Discussions

In this section, we report the results for different simulation tests performed on the tree-shaped solar cell. Before presenting the application of the proposed methodology, we discuss the details related to this test

Table 1: Performance statistics for the ideal device, the fabricated device [7] and various cases for the tree-shaped OPV cell modeled using different metallization patterns.

| Parameter                      | Ideal case | Fabricated [7] | Modeled | Case I | Case II |
|--------------------------------|------------|----------------|---------|--------|---------|
| $J_{sc}$ (mAcm <sup>-2</sup> ) | 6.14       | 2.80           | 2.76    | 2.92   | 3.22    |
| $V_{oc}$ (volts)               | 0.56       | 0.46           | 0.47    | 0.47   | 0.48    |
| $J_{mp}$ (mAcm <sup>-2</sup> ) | 5.24       | 1.45           | 1.67    | 1.88   | 2.31    |
| $V_{mp}$ (volts)               | 0.38       | 0.26           | 0.25    | 0.3    | 0.28    |

Table 2: Model parameters for the Christmas tree

| Parameter                | Value                              |
|--------------------------|------------------------------------|
| Device area              | 6.24 cm <sup>2</sup>               |
| Front PEDOT conductivity | $2 \times 10^4$ Sm <sup>-1</sup>   |
| Front PEDOT thickness    | 100 nm                             |
| Front metal conductivity | $6.3 \times 10^6$ Sm <sup>-1</sup> |
| Front metal thickness    | 300 nm                             |
| Rear PEDOT conductivity  | $5 \times 10^4$ Sm <sup>-1</sup>   |
| Rear PEDOT thickness     | 200 nm                             |
| Rear metal conductivity  | $6.3 \times 10^6$ Sm <sup>-1</sup> |
| Rear metal thickness     | 300 nm                             |

case.

Fig. 2(a) shows the schematic representation of the Christmas tree shaped free-form solar cell and photograph of the finished layout is shown in Fig. 2(b). All the functional layers, including the electrodes, were inkjet printed [7]. Inkjet printed devices contained the following layer sequence: glass substrate/front Ag fingers/front PEDOT:PSS/ZnO/ Photoactive layer/rear PEDOT:PSS/rear Ag fingers. The photoactive layer used here is Poly(3-hexylthiophene) - (P3HT) with an optical energy bandgap of around 1.7 eV. Ag fingers and busbars (both front and rear) were inkjet printed using a Fujifilm Dimatix Materials Printer (DMP 2831). Inkjet printing of front PEDOT:PSS, ZnO nanoparticles, the photo-active layer and rear PEDOT:PSS was performed on a LP50 printing platform (Pixdro, OTB) using an industrial printhead (KM512LN, 3.5 cm width, 360 DPI nozzle spacing). The specification of materials, ink formulations and inkjet printing process is described elsewhere [7]. The active area of the cell was 6.24 cm<sup>2</sup>. Fig. 2(c) and (d) show the metallization designs for the front and rear side of the free-form solar cell as were used in this study to model the electrical behaviour. These designs were obtained by a best effort based on intuition to maximize performance. Therefore, losses can be expected due to the non-optimal arrangements and thicknesses of the various electrode lines.

In this paper, we optimize the front and rear metallizations for this free-form solar cell so that its performance can be improved. For modeling purpose, we use experimental J-V data which was measured on a small device (area 0.04 cm<sup>2</sup>). The J-V curve obtained by fitting a cubic polynomial in the experimental data is as follows:

$$J(\text{mAcm}^{-2}) = -6.14 + 4.72V - 43V^2 + 97.88V^3. \quad (14)$$

The measured data as well as the fitted J-V curve are shown in Fig. 3. The proposed front-rear electrode model uses voltage values between 0.2 and 0.55 volts only. Due to this reason, only this part of the experimental data is used in Fig. 3 to derive the J-V curve. This JV-curve is then used in the front-rear electrode model for optimization.

Before optimizing the metallization patterns, we tune the model so that the behavior of the study example can be properly modeled. For the same purpose, the photoillumination component of current density in Eq. 14 is reduced by a certain factor. For a OPV, photocurrent is observed to be voltage-dependent [31–33] and this behavior is especially prominent in the reverse regime. Since our model uses the data only for a small range of positive voltage values, we assume that photocurrent is independent of voltage. Thus, the magnitude of  $J_L$  in Eq. 14 is 6.14 mAcm<sup>-2</sup>. This assumption does not affect the conclusions of this paper due to the fact that all performance related comparisons of the optimized designs are done with the modelled

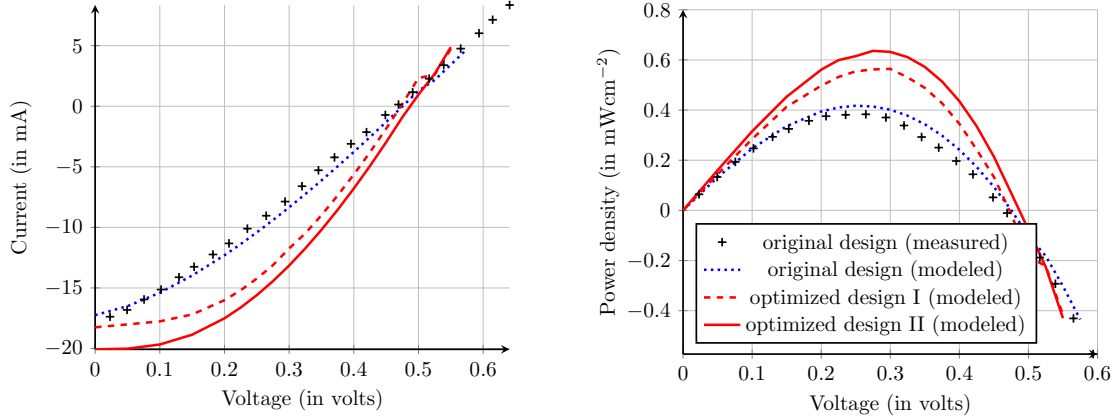


Figure 4: I-V and P-V curves for the modeled solar cell with Christmas tree shape.

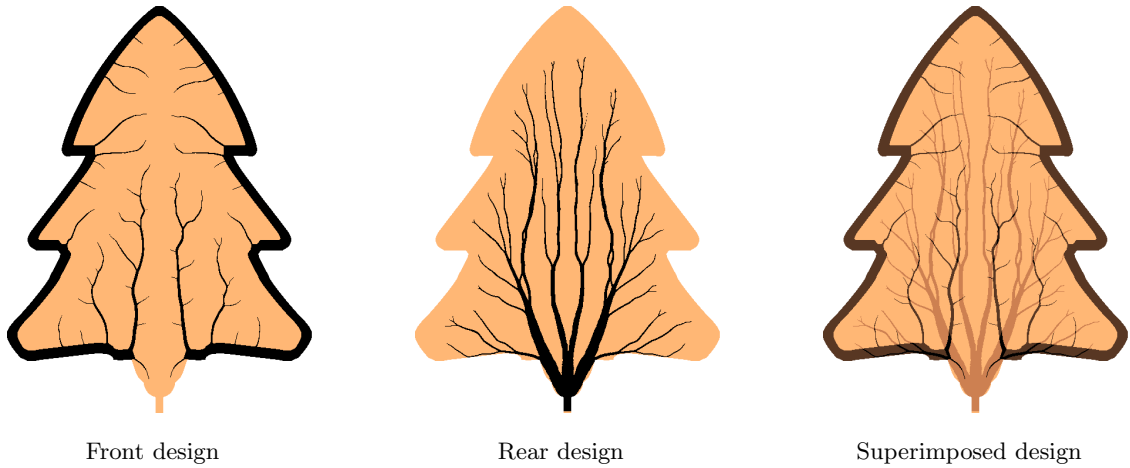


Figure 5: Optimized metallization patterns with a pre-defined perimeter electrode for the front side for a solar cell with Christmas tree shape.

version and not directly the fabricated one for the tree-shaped solar cell.

Table 2 lists the parameters used for modeling purpose. These parameters are the same as that of the previously fabricated solar cell. The PEDOT and electrode material are used to model the front and rear conductive surfaces. The effective conductivities  $G_{min}$  and  $G_0$  for every finite element stated in Eq. 7 are calculated using the information stated in Table 2 for PEDOT and electrode material, respectively. The electrode finger width is not allowed to be less than  $150 \mu\text{m}$ . Since the main goal of this paper is to present the potential of the proposed optimized strategy, we preferred to keep the model simple and certain factors have not been taken into account. An example is the transparency of the solar cell. The small device on which the J-V measurements were done consisted of an ITO layer. On a other hand, the tree-shaped solar cell discussed here uses PEDOT layer as the conductive polymer due to which its transparency is significantly lower, thereby lowering its  $J_L$ . Another factor is that the dimensions of the electrode lines in the fabricated design are generally higher than the modeled ones. This is because during inkjet printing, the ink spreads and makes shading larger [34]. Also, additional resistances including the shunt resistance have not been considered here. To include these effects in the model,  $J_L$  has been reduced by 35%. This reduction factor has been chosen ensuring that the I-V and P-V curves obtained from the model for the study device closely match those of the fabricated version.

As a next step, we use TO to optimize the front and rear metal grids for the chosen free-form solar cell. The busbar connection points are chosen to be the same as the ones in [7]. For the first instance of optimization (Case I), a fixed electrode line is defined along the perimeter of the domain for the front side.

Table 3: Performance statistics for the tree-shaped solar cell model with different metallization patterns.

| Model    | Power density (in $\text{mWcm}^{-2}$ ) | Relative Improvement |
|----------|--|----------------------|
| Original | 0.416                                  | -                    |
| Case I   | 0.564                                  | 35%                  |
| Case II  | 0.632                                  | 52%                  |

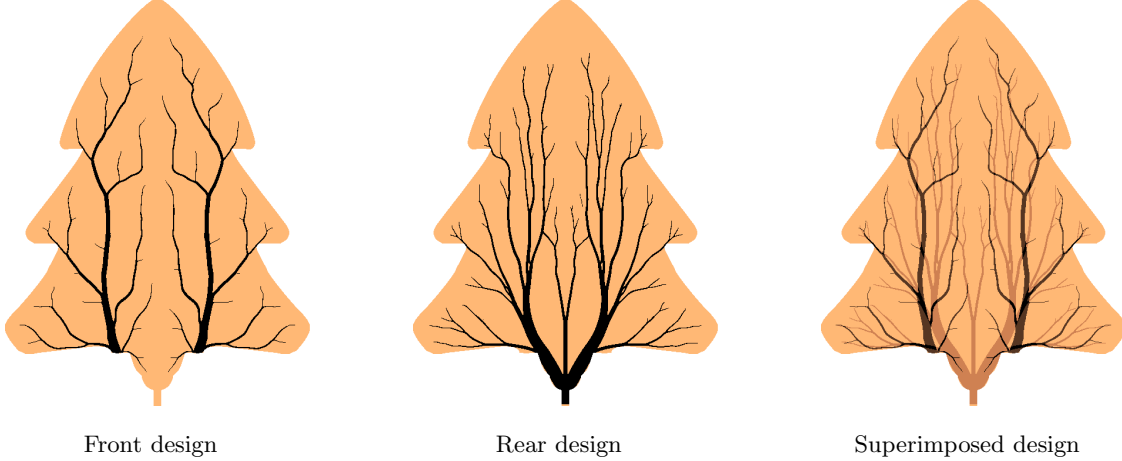


Figure 6: Fully optimized metallization patterns for a solar cell with Christmas tree shape.

The thickness of this line is kept roughly the same as the one in the original prototype cell (Fig. 2(c)). For the rear side, the amount of electrode material to be used has been set to 12% to match the original design (Fig. 2(d)) and no restriction is imposed on the amount of material to be used on the front side. Fig. 5 shows the resultant front and rear metallization patterns obtained using TO. The predefined electrodes on the perimeter of the cell already give a relatively low voltage contrast within the domain. The optimization process has only added a few small lines on the front side for further improvement and a total of 16% of the front side is found to be covered with electrode material in the optimized design. The corresponding I-V and P-V curves are shown in Fig. 4. The resultant design improves the solar cell performance by around 35% compared to the original design. Interestingly, the dendritic nature of these optimized patterns may be perceived as aesthetically appealing, ‘natural’ features. Other associated parameters such as short-circuit current density  $J_{oc}$ , open-circuit voltage  $V_{oc}$  and current density and voltage at maximum power point,  $J_{mp}$  and  $V_{mp}$ , respectively are reported in Table 1. Compared to the ideal case, significant drops are observed in  $J_{sc}$  and  $J_{mp}$  for the tree-shaped solar cell. One of the primary reasons is the shading caused due to electrode deposition on the front side. Also, since the current generated in the active layer depends on the voltage value, considerable reduction can be observed in the total current generated due to the voltage contrast on the front surface eventually leading to reduction in  $J_{sc}$  and  $J_{mp}$  of the device.

In another run of TO (Case II), no pre-defined geometry is assumed for electrode lines on the front and rear sides. Instead, it is left to the optimization process where to place all of the front electrode material. Fig. 6 shows the optimized metallization patterns obtained for this case. For this case, only 7% of the front surface of the optimized design is covered with the electrode material. The corresponding I-V and P-V curves are shown in Fig. 4 and other related parameters are reported in Table 1. With these optimized electrode patterns, a significantly higher amount of current can be collected at the busbar and a relative increase of 52% is observed in the solar cell power output. The optimal value of  $V_{bus}$  for both the cases was around 0.3 volts. Similar to the previous case, a dendritic network of electrode material is obtained for the rear side. However, a very different metallization pattern is obtained for the front side with quite a larger amount of electrode material being added during the optimization process to form the optimized pattern. The relative improvement in the solar cell performance for this case is significantly higher compared to Case I. This is because, with no pre-defined geometry here, the optimization process has more flexibility to distribute the electrode material.

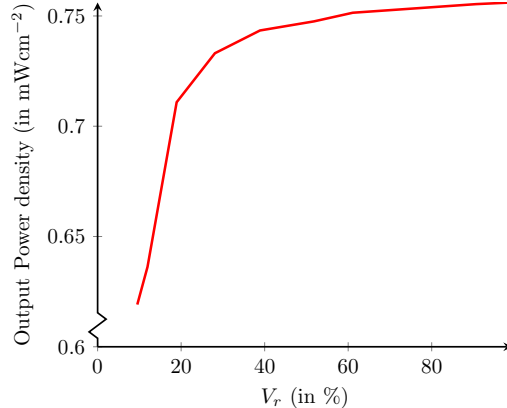


Figure 7: Solar cell power outputs for different electrode material volume fractions for the rear side of the cell.

An interesting observation is that the metallization pattern on the front side is not as densely branched as the rear side. For Case I, assuming a pre-defined geometry leaves very less amount of electrode material to be distributed on the front surface. For Case II, the amount of electrode material used on the front side ( 7%) is still quite low compared to that used on the rear side ( 12%). Due to this and the fact that a minimum feature-size restriction is imposed, the formation of a dense metallization network is avoided on the front side. Note that the choice of using 12% electrode material on the rear side was made to match the original design. It is of interest to study the influence of this choice on the optimized output power.

Fig. 7 shows the output power of different optimized metallization designs for Case II obtained for various electrode material fractions on the rear side ( $V_r$ ). With an increase in  $V_r$ , the overall power output increases. This is because the surface conductivity on the rear side increases thereby leading to a more uniform voltage distribution as well as reduced resistive losses. Thus, ideally the whole rear side should be covered with electrode material to achieve maximum performance. However, from an aesthetic point of view, these cells need to be (partially) transparent. Thus, a restriction is imposed on the value of  $V_r$ . It is interesting to see in Fig. 7 that with  $V_r$  set to 12%, the transparent Case II design, at  $0.63 \text{ mWcm}^{-2}$  achieves nearly 82% of the output power density of a fully covered cell.

From the two cases analyzed above, it can be deduced that the proposed modeling and optimization strategies work well with the chosen free-form organic solar cell example. However, the application of this methodology is not restricted to organic solar cells only. Through the use of appropriate parameter values, the proposed solar cell model can be adapted to any kind of solar cells, which allows the optimization methodology to be applied to those technologies as well. An important assumption in the applied model is that the current through the active layer runs in transverse direction. This assumption is valid for all solar cells where conductivity of front and rear surfaces is significantly higher than that of the active layer. Since this is true for most of the solar cells, our approach can be generalized and is applicable to different types of solar cells.

The goal of this paper is to demonstrate the application of the proposed optimization methodology and the presented example very well augments it. The advantages of using OPVs and the inkjet printing technique for freeform solar cells are already discussed in [7]. However, to ensure maximum power output from these freeform solar cells, several additional factors need to be considered. The power output of these cells can be affected due to the grid thickness as well as shading degradation [35]. The affect of these parameters has been studied in [36]. In [37], the effect of conductivity on the performance of thin-film solar cells has been studied. It is also important to understand the effect of stress distribution on the delamination of these solar cells and the impact that it would eventually have on their performance. Also, while modeling and optimization of the grids, we ignored the effect of temperature. The local current generated in the active layer also depends on the temperature distribution. Thus, the metallization pattern should ideally be optimized with respect to the temperature as well. In our future research work, we aim to include these aspects to further improve the accuracy of the results.

## 4 Conclusions

In this paper, a front-rear electrode model is presented which can be used to model the front and rear metallizations in solar cells. The model has been validated through comparisons with previous experimental results. Further, combining topology optimization with this model can generate front and rear metallization designs which perform significantly better than the existing ones. The application on a free-form Christmas tree shaped solar cell domain demonstrates the fact that this approach is not restricted to standard solar cell shapes and can be easily applied to free-forms. As it is nontrivial to design metallization patterns for free-form solar cells by hand, significant improvements in output power can be achieved: more than 50% for the considered example. It was also found that although efficiency of a semi-transparent cell was less than that of a full coverage rear electrode, through optimization the difference was only 18%. We expect that the proposed methodology can be a significant contribution to the trend towards transparent, free-form solar cell devices.

## Acknowledgment

This work is part of the Industrial Partnership Programme (IPP) ‘Computational sciences for energy research’ of the Foundation for Fundamental Research on Matter (FOM), which is part of the Netherlands Organisation for Scientific Research (NWO). This research programme is co-financed by Shell Global Solutions International B.V. We are grateful to Prof. K. Svanberg for providing the MMA subroutine and Roy Bijster and Qi Wang for their kind help.

## References

- [1] A. James, “Global PV Demand Outlook 2015:2020: Exploring Risk in Downstream Markets,” *GTM Research Reports*, 2015.
- [2] “Technology Roadmap: Solar Photovoltaic Energy,” *Energy Technology Perspectives, International Energy Agency*, 2014.
- [3] US Energy Information Administration, “Annual Energy Outlook 2015,” *Table: Electricity Generating Capacity*, <http://www.eia.gov/forecasts/aeo/data/browser/#/?id=9-AEO2015>, last visited 2016-03-23.
- [4] A. James, “US Solar Market Insight, Executive summary: 2015 Year-in-Review,” *GTM Research Reports*, 2015.
- [5] V. Shrotriya, “Organic Photovoltaics Polymer power,” *Nat. Photonics*, vol. 3, pp. 447–449, 2009.
- [6] W. Cao, Z. Li, Y. Yang, Y. Zheng, W. Yu, R. Afzal, and J. Xue, “Solar tree: Exploring new form factors of organic solar cells,” *Renewable Energy*, no. 72, pp. 134–139, 2014.
- [7] T. Eggenhuisen, Y. Galagan, A. Biezemans, T. Slaats, P. Voorthuijen, S. Kommeren, S. Shanmugam, J. P. Teunissen, A. Hadipour, W. Verhees, S. C. Veenstra, M. Coenen, J. Gilot, R. Andriessen, and P. Groen, “High efficiency, fully inkjet printed organic solar cells with freedom of design,” *J. Mater. Chem. A*, vol. 3, pp. 7255–7262, 2015.
- [8] N. Lewis and G. Crabtree (eds.), “Basic Research Needs for Solar Energy Utilization,” *Report on the Basic Energy Sciences Workshop on Solar Energy Utilization*, 2005.
- [9] A. Flat and A. G. Milnes, “Optimization of multi-layer front-contact grid patterns for solar cells,” *Sol. Energy*, vol. 23, pp. 289–299, 1979.
- [10] M. Conti, “Optimal design of front-contact metallization for photovoltaic solar cells,” *Solid State Electron.*, vol. 24, pp. 79–83, 1981.

- [11] A. R. Burgers, J. H. Bultman, A. C. Tip, and W. C. Sinke, “Metallisation patterns for interconnection through holes,” *Sol. Energ. Mat. Sol. C.*, vol. 65, pp. 347–353, 2001.
- [12] A. Antonini, M. Stefanchich, D. Vincenzi, C. Malagu, F. Bizzi, A. Ronzoni, and G. Martinelli, “Contact grid optimization methodology for front contact concentration solar cells,” *Sol. Energ. Mat. Sol. C.*, vol. 80, pp. 155–166, 2003.
- [13] L. Wen, L. Yueqiang, C. Jianjun, C. Yanling, W. Xiaodong, and Y. Fuhua, “Optimization of grid design for solar cells,” *J. Semicond.*, vol. 31, pp. 1–4, 2010.
- [14] Y. Galagan, E. W. C. Coenen, R. Abbel, T. J. van Lammeren, S. Sabik, M. Barink, E. R. Meinders, R. Andriessen, and P. W. M. Blom, “Photonic sintering of inkjet printed current collecting grids for organic solar cell applications,” *Org. Electron.*, vol. 14, pp. 38–46, 2013.
- [15] D. K. Gupta, M. Langelaar, M. Barink, and F. van Keulen, “Topology Optimization: An effective method for designing front metallization patterns of solar cells,” in *Proceedings, 40th IEEE Phot Spec Conf*, 2014, pp. 2471–2475.
- [16] M. P. Bendsøe and O. Sigmund, *Topology Optimization: theory, methods and applications*. Springer Germany, 2003.
- [17] O. Sigmund and K. Maute, “Topology optimization approaches A comparative review,” *Struct. Multidiscip. O.*, vol. 48, pp. 1031–1055, 2013.
- [18] J. D. Deaton and R. V. Grandhi, “A survey of structural and multidisciplinary continuum topology optimization: post 2000,” *Struct. Multidiscip. O.*, vol. 49, pp. 1–38, 2014.
- [19] S. Hyun-Jun and Y. Jeonghoon, “Texturing design for a light trapping system using topology optimization,” *IEEE T. Magn.*, vol. 48, no. 2, pp. 227–230, 2012.
- [20] C. Wang, Y. Shuangcheng, W. Chen, and C. Sun, “Highly efficient light trapping structure design inspired by natural evolution,” *Sci. Rep.*, vol. 3, 2013.
- [21] M. Otomori, T. Yamada, K. Izui, S. Nishiwaki, and N. Kogiso, “Level set-based topology optimization for the design of light-trapping structures,” *IEEE T. Magn.*, vol. 50, no. 2, 2014.
- [22] D. K. Gupta, M. Langelaar, M. Barink, and F. van Keulen, “Topology optimization of front metallization patterns for solar cells,” *Struct. Multidiscip. O.*, vol. 51, pp. 941–955, 2015.
- [23] —, “Optimizing front metallization patterns: Efficiency with aesthetics in free-form solar cells,” *Ren. Energy*, vol. 86, pp. 1332–1339, 2016.
- [24] G. M. M. W. Bissels, M. A. H. Asselbergs, J. J. Schermer, E. J. Haverkamp, N. J. Smeenk, and E. Vlieg, “A genuine circular contact grid pattern for solar cells,” *Prog. Photovolt. Res. Appl.*, vol. 18, pp. 517–526, 2011.
- [25] M. A. Green, *Solar Cells: Oper Princ Tech Sys Appl*. Prentice Hall, 1981.
- [26] D. K. Gupta, M. Langelaar, F. van Keulen, and M. Barink, “Topology Optimization for improving the performance of solar cells,” in *Proceedings, 2014 Eng. Optim Conf*, 2014.
- [27] M. P. Bendsøe, “Optimal shape design as a material distribution problem,” *Struct. O.*, vol. 1, no. 4, pp. 193–202, 1989.
- [28] M. Stople and K. Svanberg, “An alternative interpolation scheme for minimum compliance topology optimization,” *Struct. Multidiscip. O.*, vol. 22, pp. 116–124, 2001.
- [29] K. Svanberg, “The method of moving asymptotes - a new method for structural optimization,” *Int. J. Numer. Meth. Eng.*, vol. 24, pp. 359–373, 1987.

- [30] F. van Keulen, R. T. Haftka, and N. H. Kim, “Review of options for structural design sensitivity analysis. Part 1: linear systems,” *Comput. Method. Appl. M.*, vol. 194, pp. 3213–3243, 2005.
- [31] L. J. A. Koster, E. C. P. Smits, V. D. Mihailtchi, and P. W. M. Blom, “Device model for the operation of polymer/fullerene bulk heterojunction solar cells,” *Phys. Rev. B*, vol. 72, pp. 085 205–1–9, 2005.
- [32] L. H. Slooff, S. C. Veenstra, J. M. Kroon, W. Verhees, L. J. A. Koster, and Y. Galagan, “Describing the light intensity dependence of polymer:fullerene solar cells using an adapted Shockley diode model,” *Phys. Chem. Chem. Phys.*, vol. 16, pp. 5732–5738, 2014.
- [33] B. Ray, A. G. Baradwaj, M. R. Khan, B. W. Boudouris, and M. A. Alam, “Collection-limited theory interprets the extraordinary response of single semiconductor organic solar cells,” *Proc. Natl. Acad. Sci. USA*, vol. 112, no. 36, pp. 11 193–11 198, 2015.
- [34] Y. Galagan, R. Andriessen, E. Rubingh, N. Grossiord, P. Blom, S. Veenstra, W. Verhees, and J. Kroon, “Toward fully printed organic photovoltaics: processing and stability,” *Lope-C*, p. 8891, 2010.
- [35] S. Dongaonkar and M. A. Alam, “Geometrical design of thin film photovoltaic modules for improved shade tolerance and performance,” *Prog. Photovol: Res. Appl.*, vol. 23, pp. 170–181, 2015.
- [36] Y. Galagan, E. W. C. Coenen, S. Sabik, H. H. Gorter, M. Barink, S. Veenstra, J. Kroon, R. Andriessen, and P. Blom, “Evaluation of ink-jet printed current collecting grids and busbars for ITO-free organic solar cells,” *Sol. Energ. Mat. Sol. C.*, vol. 104, pp. 32–38, 2012.
- [37] Y. Galagan, B. Zimmerman, E. W. C. Coenen, M. Jorgensen, D. M. Tanenbaum, F. C. Krebs, H. Gorter, S. Sabik, L. H. Sloff, S. Veenstra, J. Kroon, and R. Andriessen, “Current collecting grids for ITO-free solar cells ,” *Adv. Energy Mater.*, vol. 2, no. 1, pp. 103–110, 2012.